Ahmed Azzam[1,2], Wei Li[1]*

Experimental Investigation on the Impact Behaviour of Composite Laminate

[1)]**College of Textiles, Donghua University,**
Shanghai 201620, China
Corresponding author: liwei@dhu.edu.cn

[2)]**School of Engineering and Technology Industries, Department of the Textile Engineering, Sudan University Science and Technology,**
Khartoum, Sudan

Abstract
The impact response of a composite laminate structure was investigated by subjecting several stacking sequences of a composite laminate structure to low velocity impact loading using a Drop-Weight Machine (CEAST 9350 drop tower) and three-point bending using an electronic universal tester (Type: WDW-20) machine. The air-coupled ultrasonic C-scan technique (NAUT21) was selected in order to characterise the impact damage size, delamination, flaw detection, and damage in composite laminate structures. The failure processes of damaged specimens for impact energy (5 J) were evaluated by comparing load-displacement curves and images of damaged samples taken from impacted sides through a C-scan.

Key words: *stacking sequences, low velocity impact, C-scan, three- point bending, delamination.*

Introduction

Composite materials have been competitive alternatives to traditional metallic materials for a while due to their lower density, higher stiffness, higher strength, and better fatigue resistance when compared to steel or aluminum. Such properties enable composites to be an ultimate candidate for structural applications in aerospace and automotive products. Carbon fibre reinforced plastics (CFRP) with laminated structures are one of the most concerned types of composites, thus attracting researcher's attention for the last two decades. The incentives to study the impact damage inspection strategies of CFRP laminated structures are not only due to the increase in their demand, but also because of the fact that CFRP structures suffer more severely from such damage than other composite materials [1]. The use of a three-point support flexural test to predict the stiffness of anisotropic composite plates in bending was studied by Nunes et al. The results show that the flexural behaviour of the composites depends on several factors, such as fibre orientation, laminate stacking, surface waviness and molding temperature [2]. Many studies have been carried out on bending properties of composite laminate by considering several factors, such as fibre orientation, laminate stacking, and manufacturing conditions [3 - 9]. Ultrasonic testing has been used for years as a method of examining parts and components in production, as a means of verifying product quality and for inspecting service parts for damage and defects [10]. Increased usage of FRP challenges non-destructive testing (NDT). Detection of the large variety of defects occurring in heterogeneous and anisotropic polymer-matrix composites during their manufacturing process and operation requires advanced non-destructive evaluation (NDE). For example, fatigue damage of metals is characterised by the nucleation and growth of a single crack, which is detectable using conventional penetrant or eddy current testing. In comparison, the fatigue mechanisms of (frequently non-conducting) FRP involve many different defects and more complex accumulation of damage [11]. Various non-destructive testing (NDT) modalities, such as X-ray CT, thermography, ultrasonic, acoustic emission, etc., have been used to detect and identify damage types in composites. Over the last 20 - 30 years, there has been significant work performed in experimental ultrasonic testing to detect and characterise damage modes in composites [12 - 14]. The development of nondestructive inspection techniques has been remarkable in many industries, where the defect inspection system plays a key role. Among such inspection systems, the nondestructive techniques examine the physical properties and defects of a sample without destroying it. Non-contact air coupled ultrasonic testing has been used to detect damage in composite structures and also employed to inspect a sample with rough surfaces or those with very low or high temperature. It has also been used where the conventional contact ultra-sonic testing method cannot be employed due to the difficulty of applying a coupling in constricted spaces. The technique is used to detect the decay and defects of material with very high or low temperature, or to inspect curved surfaces of air-craft and the delamination of carbon composite material used for automobiles [15]. The NAUT21 detection system can be used for composite material, lithium ion batteries, brake pads, ceramic materials, concrete, wood, rubber, plastic and other materials. The air-coupled approach has

Table 1. *Mechanical properties of composite laminate.*

Young modulus (longitudinal), GPa	E_1 = 135.0
Young modulus (transverse), GPa	E_2 = 8.91
Shear modulus, GPa	G_{12} = 98
Poisson ratio	v = 0.3
Ply thickness, mm	t = 0.125

(length × width). ***Table 1*** represents calculated mechanical properties of the lamina produced.

The mechanical properties of composite lamina calculated by the following equations:

$$E_1 = E_f V_f + E_m V_m \quad (1)$$

$$\frac{1}{E_2} = \frac{V_f}{E_f} + \frac{V_m}{E_m} \quad (2)$$

$$\frac{1}{G_{12}} = \frac{V_f}{G_f} + \frac{V_m}{G_m} \quad (3)$$

$$\upsilon_{12} = \upsilon_f V_f + \upsilon_m V_m \quad (4)$$

where, E_1 is the longitudinal stiffness, E_f and E_m the stiffness of fibre and matrix, V_f and V_m the he volume fraction of fibre

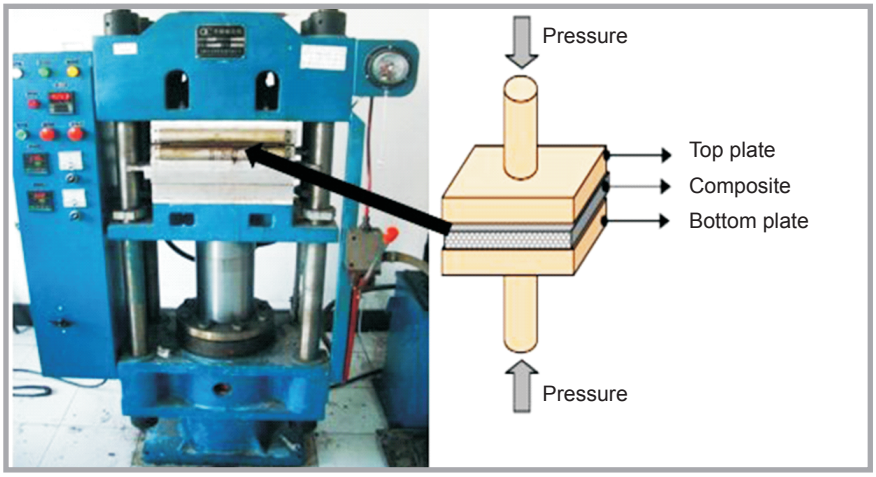

Figure 1. *Compression molding machine (flat-panel vulcanizer).*

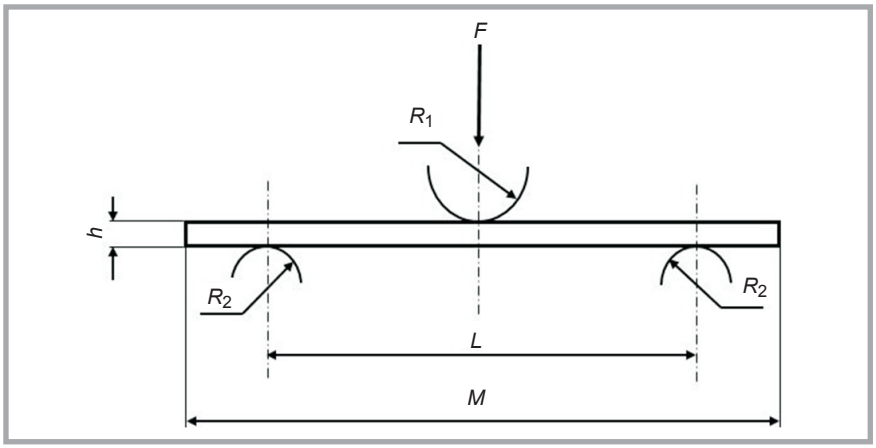

Figure 2. *Load configuration for a beam in three point bending; F is the applied force, R_1 - indenter radius, R_2 - fixed support radius, h - specimen thickness, L - support span and M - specimen length.*

Table 3. *Specimen characteristics and specifications; Qu - denotes to quasi-isotropic, Un - denotes to unbalance.*

Laminate type	Specimen name	Lay-up, degrees	N of plies	Span L, mm	Width b, mm	Specimen length M, mm	Specimen thickness h, mm
Quasi-isotropic stacking sequence	Qu1	$[0/90/-45/45]_{2s}$	16	40	15	70	2
	Qu2	Same	16	40	15	70	2
	Qu3	Same	16	40	15	70	2
Unbalance stacking sequence	Un1	$[45/45/90/0]_{2s}$	16	40	15	70	2
	Un2	Same	16	40	15	70	2
	Un3	Same	16	40	15	70	2

Table 2. *Testing equipments.*

Number	Name	Model
1	Electronic universal tester	WDW-20
2	Optical microscope	Nikon eclipses E200
3	Impact tester (Instron)	CEAST 9350
4	C-scan	NAUT21

a great advantage in the case of composite materials as C-scan observations help in determining the shape of the different delamination and their locations in the composite plates [16]. Most previous air-coupled ultrasonic investigations were based on the through-transmission and pitch-catch configuration of transducers [10, 17 - 20]. Air-coupled ultrasonic testing presents subtle challenges to the engineer seeking to employ this technique for defect detection or materials characterisation [21]. In current studies, the impact, bending, and C-scan of the laminate composite structure was investigated. Two types of stacking sequence were chosen for the bending test: $[0/90/-45/45]_{2s}$ call quasi-isotropic and $[45/45/90/0]_{2s}$ call unbalance stacking sequence and s denotes to symmetric. Also four types of stacking sequences were chosen for the impact property: $[0/90/-45/45]_{2s}$, $[45/45/90/0]_{2s}$, $[0/90/-45/45]_s$ and $[45/45/90/0]_s$ to characterise impact damage in the composite laminate structures. A non-destructive technique was used to detect the delaminated area of the specimens. A laminate composite structure with different stacking sequences was evaluated on an Instron CEAST 9350 impact tester (Instron Company, United States & Canada). The effects of the stacking sequence were used and being discussed.

Materials and methods

Materials

T700S-24k carbon fibre/epoxy unidirectional Prepreg produced by the Torayca Company (Toray Carbon Fibers, China) was used to manufacture composite laminates.

Laminates fabrication

Laminates fabrication which consist of four different stacking sequences was prepared by the compression molding composite process as shown in ***Figure 1***. The pressure was 2 MPa; curing lasted 30 min at 80 °C, and post-curing for 120 min at 120 °C. The dimensions of the entire sample were 16 × 16 cm

and matrix, E_2 the transverse stiffness, G_{12} the shear modulus, G_f and G_m the shear modulus of fibre and matrix and υ_f, υ_m the Poisson ratio of fibre and matrix. The testing equipment used in the experiments included an electronic universal tester (Type: WDW-20) machine (Shanghai HUALong WDW Series, China), optical microscope (Nikon eclipses E200, Japan), non-contact air coupled ultrasonic testing (NAUT21, Japan Probe Co, Ltd), and a CEAST 9350 drop tower (Instron), see ***Table 2***.

Three point bending test

Three-point bending test was conducted with an electronic universal tester (Type: WDW-20) machine. The velocity of the bending load applied was 2 mm/min. ***Figure 2*** shows the load configuration for a beam in the three point bending tests. Different stacking sequences laminate types were tested, firstly quasi-isotropically and secondly in an unbalanced stacking sequence. Load–displacement plots were obtained for each test specimen, and three specimens of each type of composite laminate were tested. ***Table 3*** shows the lay-up, number of plies and dimensions for each specimen. The dimensions and all the procedures for the three-point bending test were set according to Standard (ISO14125:1998, Fibre-reinforced plastic composites-determination of flexural properties N EQ). The flexural stress Q_f is given by the following equation:

$$Q_f = \frac{3FL}{bh^2} \tag{5}$$

where,

Q_f - flexural stress, in MPa;
F - load in N;
L - span, in mm;
h - thickness of the specimen, in mm;
b - width of the specimen, in mm.

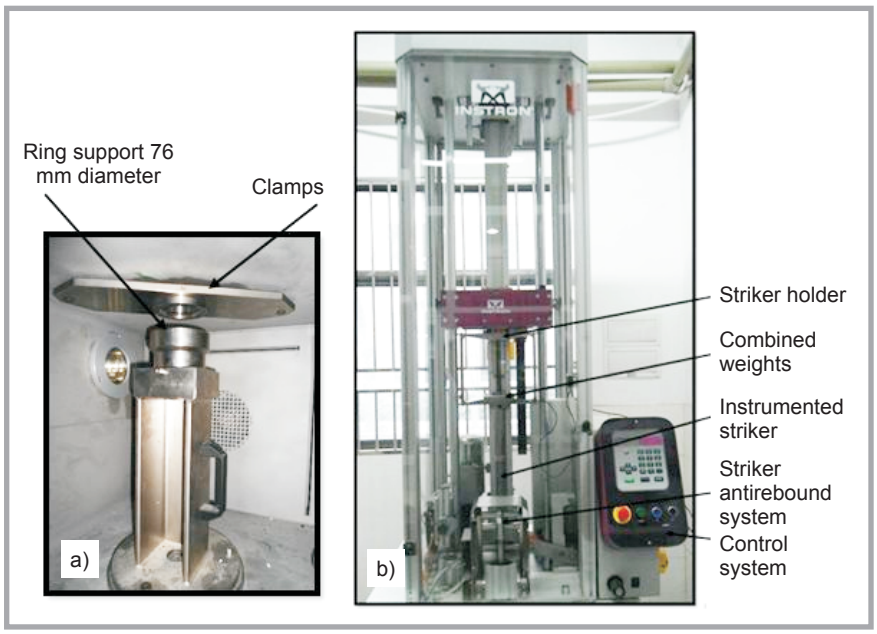

Figure 3. *CEAST 9350 impact tester: (a) test chamber, and (b) device system.*

Impact testing

An INSTRON CEAST 9350 drop tower impact tester machine, ***Figure 3***, was used to conduct the impact test. The test was performed by dropping a 16 mm diameter hemispherical striker with 5.277 kg weight on the specimens from various heights. The striker weight includes a carriage weight of 4.3 kg, a striker of 0.63 kg and additional 0.347 kg. An impact energy of 5 J was applied to the laminates. The incident velocity was 1.38 m/s and the drop height is 96.7 mm. The tests were done according to the ASTM 7136 standard [22].

Non-contact air coupled ultrasonic testing (NAUT21)

The non-contact detection ultrasonic method was used so that a coupling agent is not required to be applied on the specimen to eliminate the risk of its contamination. The facility, NAUT21, is shown in ***Figure 4***.

The detection part is shown in ***Figure 5***. It consists of a top probe (pulser) and bottom probe (receiver) with 400 KHz frequency. The probe diameter is 20 mm.

Principle of operation procedure

Firstly put the inspection material as shown in ***Figure 5***, between the left & right clamp holders (removable to fit the sample size) and adjust the holder height to get the same distance from the sample to the pulser and from the sample to the receiver. Secondly: move the pulser & receiver devices above & below the undamaged area to get a fundamental healthy material pulse. Thirdly set the parameters (1 - continuous: to get a continuous ultrasonic transmission pulse, 2 - amplitude: initial value 20 dB for general material; increase the gain value to get enough echo amplitude and decrease the gain value if the amplitude is big, 3 - frequency: adjust the frequency to get the good waveform, which means

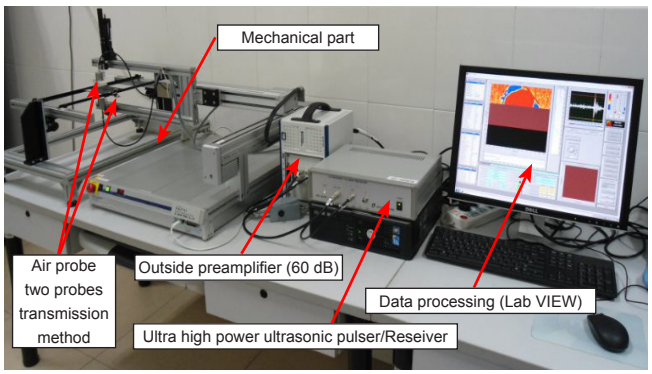

Figure 4. *Non-contact air coupled ultrasonic testing facility.*

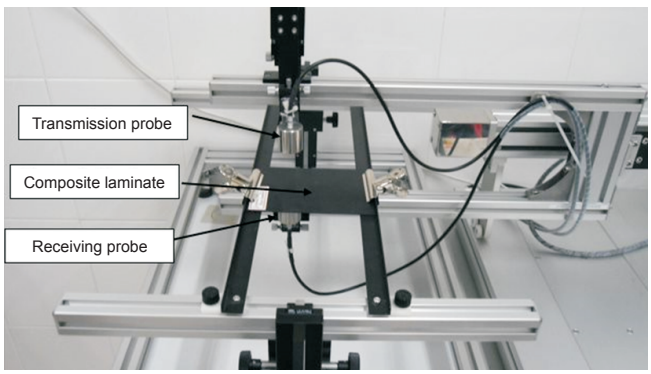

Figure 5. *Detection part with transmission and receiving probe.*

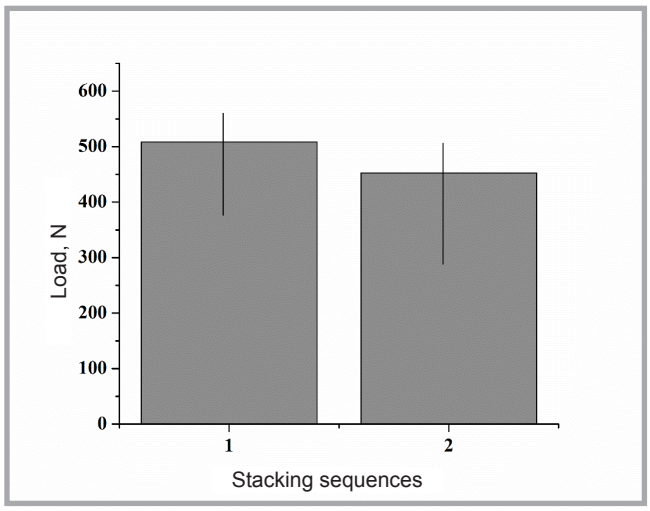

Figure 6. Mean load values in N of the stacking sequences tested.

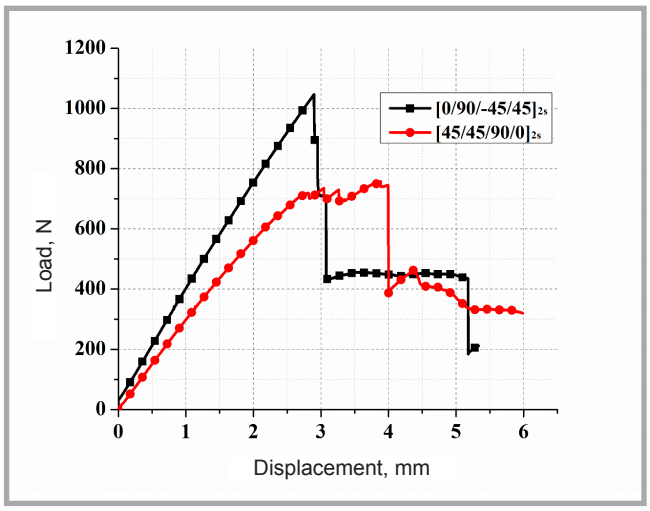

Figure 7. Electronic universal tester plot of the load vs. displacement of the composite laminate.

3 - 5 waves between the vibration starting point, 4 - measurement range: distance between adjacent measuring points and 5 - scanning speed: the moving speed of the pulsar & receiver couple). Fourthly set the measurement range by moving the stage to set the diagonal points as the start and end points, and next save the settings. Finally start scanning to get a final C-scan image.

Statistical analysis

Statistical analysis was performed with origin 8.5, and descriptive statistics were calculated (mean, standard deviation, median, minimum, and maximum values). The normality of the distributions was assessed with Kolmogorov and Smirnov test. A multifactor analysis of variance (ANOVA) was applied to determine whether there were significant differences among the various stacking sequences. The Tukey post hoc test was applied [23]. Significance for all statistical tests was predetermined at $P < 0.05$.

Results and discussion

Three point bending testing

This section describes the experimental results after the various composite samples were broken under three point bending (initial delamination, matrix crack, fibre crack). All results are plotted in terms of the load applied versus the center displacement of the sample under the crosshead of the electronic universal tester machine. All the samples for two stacking sequences had the same span length, thus making it possible to superimpose the load/displacement plots for each group of samples. This allows for a more accurate comparison of the resulting curves. In each case there is reasonably good correlation in the results. For these samples the failure mechanism observations are reproducible.

Laminate: $[0/90/-45/45]_{2s}$

Figure 7, illustrates load-displacement plots for laminates composite structures of $[0/90/-45/45]_{2s}$ consisting of 16 layers. Observations of the behaviour of the composite laminate under bending stiffness were made during the test until the peak load of the laminate due to no delamination observed and no oscillations before the peak load, which may result from vibrations of the supports not taking place, no defects in the composite laminates, and little initiation of damage in the specimens. The curves can be divided into three regions: the first region, linear in appearance could explain the elastic deformation of the composite laminate. The deformation was noticeable when the displacement of the indenter was affected in the upper surface, due to the presence of some imperfections on the surface of the laminate. The second region after the load reached a peak value, a significant drop of about 50% in the peak load was seen and a displacement curve was observed in the composite laminate structures. This sudden drop would be due to fibre cracking. After the crack initiated in the tensile side, it propagated to the compressive side within all types of specimens before the final failure occurred. After the load drop, the specimen continued to sustain the load, but never exceeded the previous peak load as only the reinforcement carrying the load, which is reflected in the third region. In this region, a plateau region was observed until reaching final failure.

Laminate: $[45/45/90/0]_{2s}$

Figure 7 shows the behaviour of the composite laminate due to bending stiffness, delamination, and oscillations during the test until the peak load in the laminate. This stacking sequence showed a few oscillations before the peak load, which may result from vibrations of the supports, some defects in the composite laminates, dents and delamination on the top and bottom face of the laminate composite structure, and initiation of damage in the specimens. The curves are divided into three regions. The first region, linear in appearance could explain the elastic deformation of the composite laminate. The second region after the load reached a peak value, the failure behaviour is similar to other laminate. After the load drop, the specimen continued to sustain the load, but never exceeded the previous peak load as only the rein-

Table 4. Descriptive statistics, in N, of maximum flexural strength values of the stacking sequences tested.

Number	Specimen lay-up	Mean	SD	Min	Median	Max
1	$[0/90/-45/45]_{2s}$	508.36	236.24	0	450.66	1046.38
2	$[45/45/90/0]_{2s}$	452.80	200.95	0	411.51	757.56

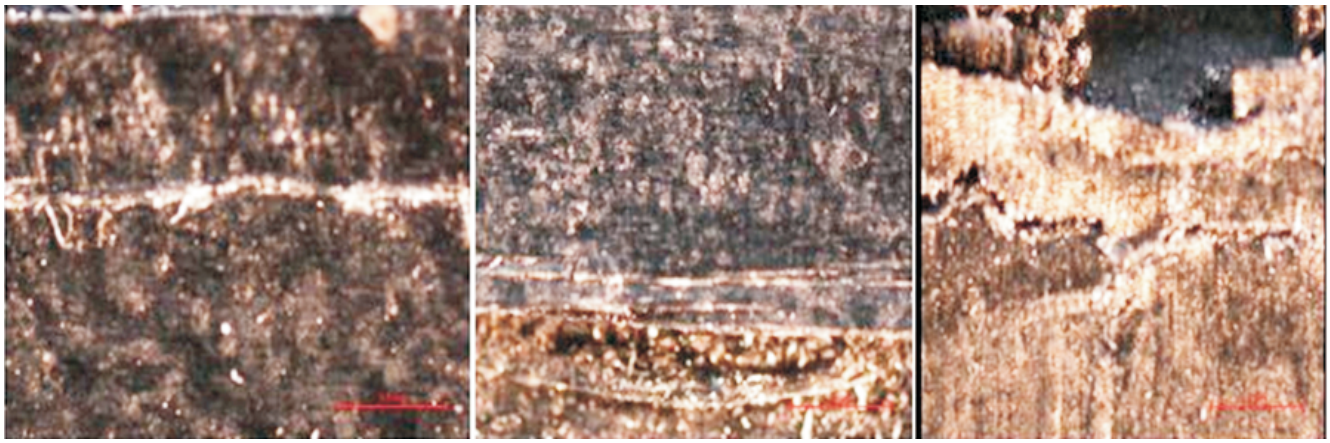

Figure 8. *Optical microscope photos for Qu1, Qu2, Qu3: [0/90/-45/45]$_{2s}$.*

Figure 9. *Optical microscope photos for Un1, Un2, and Un3: [45/45/90/0]$_{2s}$.*

forcement carrying the load, which is reflected in the third region. In this region, a plateau was observed until reaching final failure. The maximum fibre stress at failure on the tension side of a flexural specimen is considered the flexural strength of the material. By comparing the two types of stacking sequences used in this test, $[0/90/-45/45]_{2s}$ has advantages over $[45/45/90/0]_{2s}$ as it carries a high load, and has a small damage area, and no delamination due to the different lay-up, fibre orientation, and difference in their respective fibre modulus. $[0/90/-45/45]_{2s}$ exhibits brittle behaviour, but the second laminate shows a progressive failure mode consisting of fibre failure, debonding (splitting) and delamination. The $[45/45/90/0]_{2s}$ laminate has a highly nonlinear load–displacement curve due to compressive yield.

Statistical analysis results

The descriptive statistics of the maximum load of the different two stacking sequences, including mean, standard deviation, median, minimum, and maximum are shown in ***Table 4*** and ***Figure 6***. The results of ANOVA indicated significant differences among the various stacking sequences ($P < 0.001$). Post hoc test pointed out that $[0/90/-45/45]_{2s}$ showed significantly higher load values than $[45/45/90/0]_{2s}$ ($P < 0.05$).

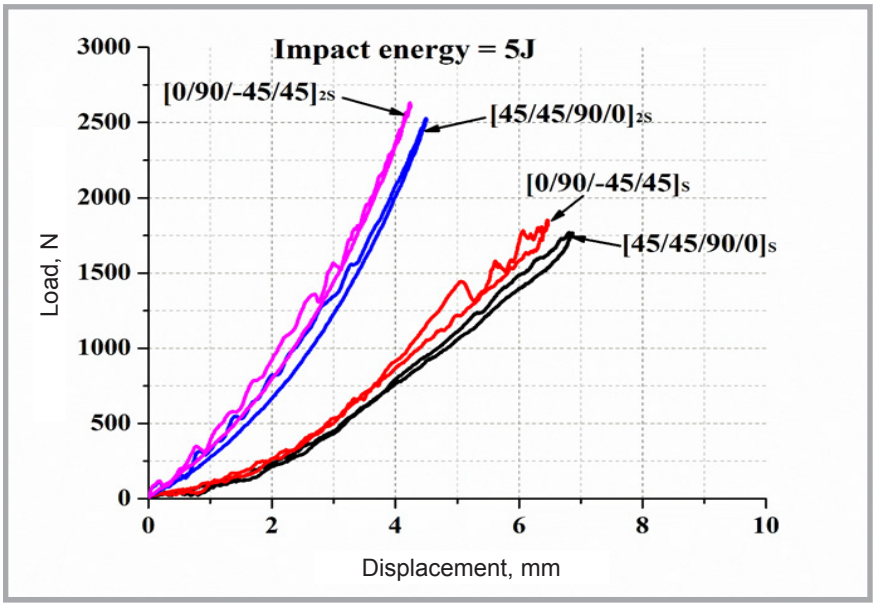

Figure 10. *Load-displacement curves for low-velocity impact tests of composite laminates.*

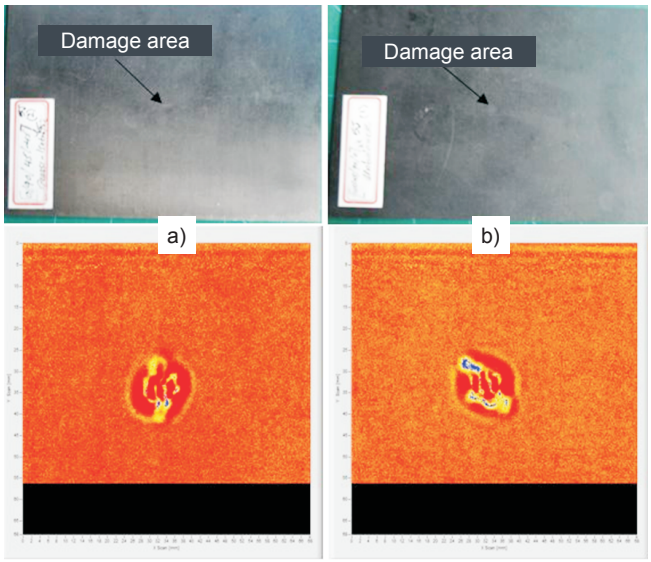

Figure 11. *Pictures of the top surfaces of laminates viewed by C-scan of: a) $[0/90/-45/45]_{2S}$, b) $[45/45/90/0]_{2S}$ at 5 J.*

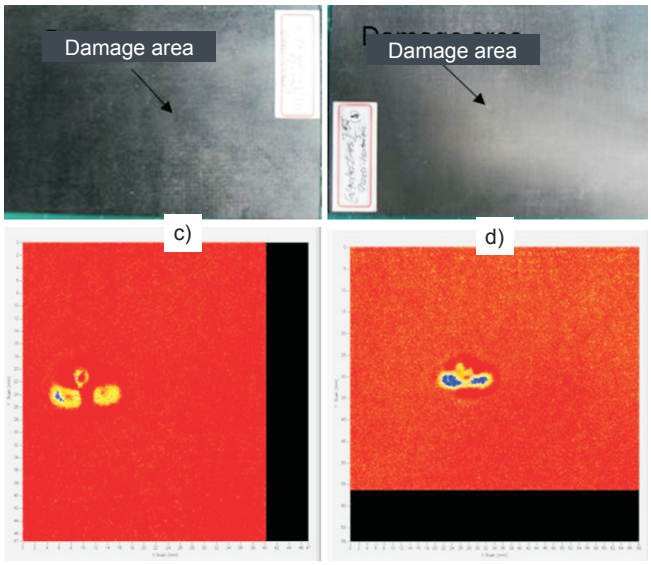

Figure 12. *Pictures of the top surfaces of laminates viewed by C-scan: c) $[0/90/-45/45]_S$, d) $[45/45/90/0]_S$ at 5 J.*

Optical microscopic images

Optical microscope results show the shapes of the failure, which occurs in the samples. A high delaminated area occurs in $[45/45/90/0]_{2S}$ with the unbalance stacking sequence due to the orientation of the layer, and fibre orientation. ***Figures 8*** and ***9*** show photos taken in the transverse direction of the composite laminates for two types of stacking sequences.

In ***Figure 8*** the photos show a small delaminated area, and a small damage area, with almost same damage shape in the upper surface of the laminate. However, in ***Figure 9***, we can see the biggest delaminated area, large damage indentation, various damage shapes, fibre failure, and debonding (splitting). Which could attributed to important role and effects of fibre orientation in composite laminates.

Impact damage testing

In this test, we selected four types of the lay-up, $[0/90/-45/45]_{2S}$, $[45/45/90/0]_{2S}$, $[0/90/-45/45]_S$, and $[45/45/90/0]_S$. The first two have 16 ply with thickness 2 mm for whole laminate and last two 8 ply with thickness 1 mm. All the composite laminates lay-ups were subjected to an impact energy of 5 J to get a full image of the impact behaviour. From ***Figure 10*** we can see that each of the two types of composite laminates lay-ups almost has the same behaviour in the case of the rebounding of the impactor to the original point graph due to the fact, that the specimens impacted by lower energy have a response that tends towards a quasi-static response. In addition to that the composite laminate still resisted damage and could carry an additional load.

In the case of a high load it was the quasi-isotropic composite laminate that reached a peak load rather than unbalance stacking sequences due to the differences in lay-up and thickness of the laminate. Individually, all the curves have an ascending section of loading, reaching a maximum load value and descending section of unloading. The ascending section of the load - displacement curve is known as bending stiffness due to the resistance of the composite to impact loading, and in this section, the maximum load reached the highest value, also known as the peak force. In the typical load - displacement curves of the composite laminates structure subjected to impact loading (5 J) rebounding was observed. Rebounding results in closed curves indicating the rebounding of the impactor from the specimen surface, and the closed type curves return back to the origin of the graph after the descending section from the peak force value as shown in all types of stacking sequences at a 5 J impact energy.

Characterization of impact damage

Failure mechanism

The impact damage mechanism in a laminate constitutes is very complex process. It is a combination of matrix cracking, surface buckling, delamination, fibre shear-out, and fibre fracture, etc., which usually all interact with each other [24]. In this study air-coupled C-scan images were obtained in order to study the possibility of determining the delaminated areas in the top and bottom surfaces of the laminate composite structure, see ***Figure 11 - 12***. C-scan techniques play an important role in detecting damage in composite structures.

Figure 11 shows images of the damage which occurred in the surfaces of composite laminates $[0/90/-45/45]_{2S}$ and $[45/45/90/0]_{2S}$ at 5 J impact energy. From the images, no internal damage can be visually detected due to their little damage indentation in the damage area. However C-scan image results show that internal damage like delamination occurs in the composite laminates, but the quasi-isotropic laminate has a smaller delaminated area than the unbalance stacking sequence laminate, attributed to the differences in lay-up, fibre orientation, and interface bonding thereof. In summary, visual detection with the non-destructive technique is not in agreement with the damage shape, damage size and delamination shown by C-scan images, which give only the overlapping delamination area directly under the impact site, whereas visual inspection of the laminate surface and macroscopic observations of the sample section show the extent of the largest, single denomination.

Figure 12 shows images of the damage which occurred in the surfaces of composite laminates $[0/90/-45/45]_S$ and $[45/45/90/0]_S$ at 5 J impact energy. The laminate consisted of 8 ply, less than the laminate in ***Figure 8***. From the images, small indentation was observed located under the striker place in surface of the

laminate. However, the C-scan technique showed the real shape and size of impact damage, as compared to C-scan images showing only the overlapping delamination area directly under the impact site. In the C-scan mode, the extent of damage or internal inhomogeneity can be examined and the depth profile of the damage can be obtained by varying the colours, which gives the exact locations of damage occurring in the top surface of the laminate composite. This method was found to be more convenient and reflected the final delaminated area with measurement of the fail area which had occurred in the composite structure.

The delaminated area in the C-scan image with blue and yellow colours shows the size and shape of delamination that occurred in the composite plates. In the C-scan image, it is more convenient to detect delamination, damage size sensitivity, damage location sensitivity, and the distance from the surface.

Fail area measurement of laminates

From ***Figure 13 - 14***, the fail area of damage progress which occurred in the composite laminates for stacking sequences $[0/90/-45/45]_{2s}$, and $[45/45/90/0]_{2s}$ were obtained from the C-scan image at 5 J impact energy.

From observations of the C-scan image, we can anticipate when the impact energy increase, the size of the damage, indentation and, delamination, as well as the fail area increase. All these measurements are conducted using a C-scan image. Compared the stacking sequences using C-scan images of $[0/90/-45/45]_{2s}$ and $[0/90/-45/45]_{s}$ the upper face has a lower fail area, delamination, indentation in the damage location, and damage size sensitivity than $[45/45/90/0]_{2s}$ and $[45/45/90/0]_{s}$. This behaviour is attributed to variation in the stacking of layers in the composite laminate, the total number of layers, the thickness of the laminate, and to the mechanical property of lamina.

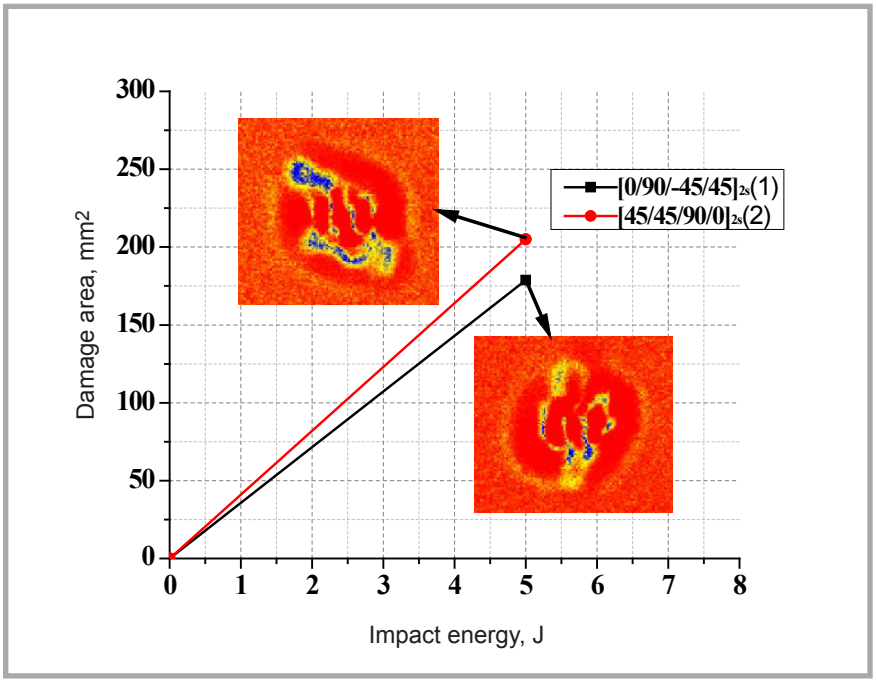

Figure 13. *Measurement of damage area to top surfaces of laminates $[0/90/-45/45]_{2s}$ and $[45/45/90/0]_{2s}$ at 5 J from the C-scan image.*

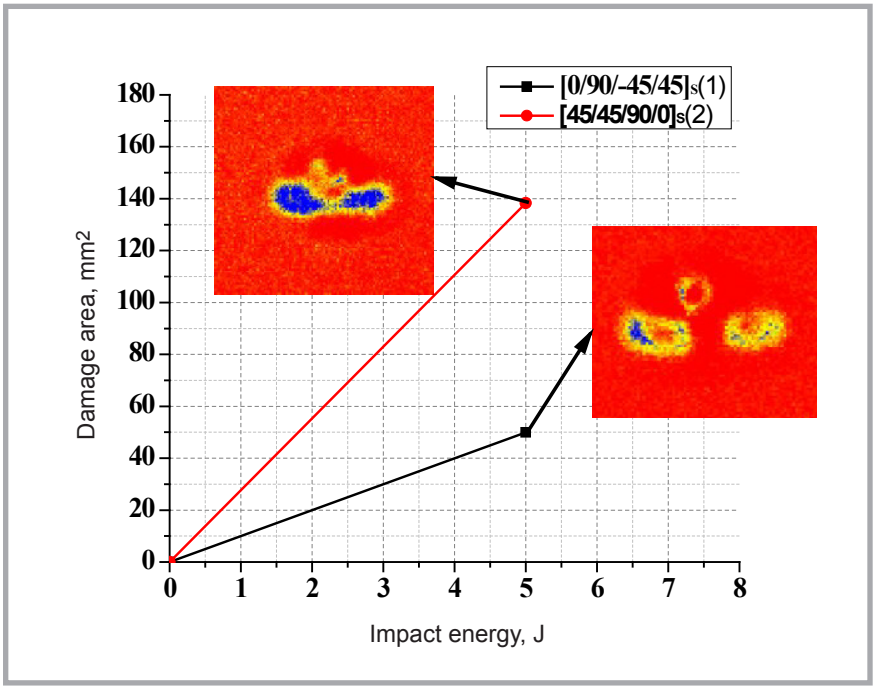

Figure 14. *Measurement of damage area to top surfaces of laminates $[0/90/-45/45]_{s}$ and $[45/45/90/0]_{s}$ at 5 J from the C-scan image.*

Conclusion

The three point-bending test and low velocity impact behaviour of composites laminates were investigated through the C-scan non-destructive method. At a 5 J impact energy, it was observed that the impactor rebounded without penetrating the specimens due to the stiffness of the laminate structures. Three point-bending results show that $[0/90/-45/45]_{2s}$ exhibits its brittle behaviour, whereas the other laminate exhibits a progressive failure mode consisting of fibre failure, debonding (splitting), and delamination. The $[45/45/90/0]_{2s}$ laminate has a highly nonlinear load–displacement curve due to compressive yielding. Compared the stacking sequences using C-scan images of $[0/90/-45/45]_{2s}$ and $[0/90/-45/45]_{s}$ the upper face has a lower fail area, delamination, indentation in the damage location, and damage size sensitivity than $[45/45/90/0]_{2s}$ and $[45/45/90/0]_{s}$. This behaviour is attributed to variation in the stacking of layers in the composite laminate, to the total number of the layers, to the thickness of the laminate, and to the mechanical property of lamina.

Acknowledgements

The authors would like to thank Tongji University for providing the impact damage and C-scan facilities located at the School of Aerospace Engineering and Applied Mechanics.

References

1. Shen Q, Omar M, Dongri S. Ultrasonic NDE Techniques for Impact Damage Inspection on CFRP Laminates. *Journal of Materials Science Research* 2012; 1.
2. Nunes J, Pouzada A, Bernardo C. The use of a three-point support flexural test to predict the stiffness of anisotropic composite plates in bending, *Polymer testing*, 2002; 21: 27-33.
3. Ary Subagia IDGK, Tijing Y, Kim LD, Shon CS, Kyong H, Effect of stacking sequence on the flexural properties of hybrid composites reinforced with carbon and basalt fibres, *Composites Part B: Engineering*, 2014; 58: 251-258.
4. Belingardi G, Cavatorta MP, Bending fatigue stiffness and strength degradation in carbon–glass/epoxy hybrid laminates: Cross-ply vs. angle-ply specimens, *International Journal of Fatigue*, 2006; 28: 815-825.
5. Carbajal N, Mujika F. Determination of longitudinal compressive strength of long fibre composites by three-point bending of [0m/90n/0p] cross-ply laminated strips, *Polymer Testing*, 2009; 28: 618-626.
6. De Baere I, Van Paepegem W, Degrieck J. Comparison of different setups for fatigue testing of thin composite laminates in bending, International *Journal of Fatigue*, 2009: 31: 1095-1101.
7. Fujihara KH, Ramakrishna Z-M, Hamada S, H. Influence of processing conditions on bending property of continuous carbon fibre reinforced PEEK composites, *Composites Science and Technology*, 2004; 64: 2525-2534.
8. Tomita Y, Morioka K, Iwasa M. Bending fatigue of long carbon fibre-reinforced epoxy composites, *Materials Science and Engineering: A*, 2001; 319–321: 679-682.
9. Vargas G, Mujika F. Determination of in-plane shear properties by three-point flexure test of±45° anti-symmetric laminates, *Polymer Testing*, 2011; 30: 204-215.
10. Peters J, Kommareddy V, Liu Z, Fei D, Hsu D. Non-contact inspection of composites using air-coupled ultrasound. In: *AIP Conference*, 2003, pp. 973-980.
11. Rheinfurth M, Schmidt F, Protz R, Busse G, Horst P, Gude M, Hufenbach W. Evaluation of Fatigue Damage in Composites with Various Defects Using Air-coupled Guided Waves, 18th World Conference on Nondestructive Testing, (2012).
12. Baste S, El Guerjouma R, Audoin B. Effect of microcracking on the macroscopic behaviour of ceramic matrix composites: ultrasonic evaluation of anisotropic damage. *Mechanics of Materials* 1992; 14: 15-31.
13. Kong HP, Zhang Z, Li LF. Factors influencing acousto-ultrasonic approach to impact damage in composite materials. *Advanced Materials Research* 2012; 393: 97-101.
14. Polimeno U, Meo M, Almond DP, Angioni SL. Detecting low velocity impact damage in composite plate using nonlinear acoustic/ultrasound methods. *Applied Composite Materials* 2010; 17: 481-488.
15. Kažys R, Demčenko A, Žukauskas E, Mažeika L. Air-coupled ultrasonic investigation of multi-layered composite materials. *Ultrasonics* 2006; 44, Supplement: e819-e822.
16. Lesser AJ. Effect of resin crosslink density on the impact damage resistance of laminated composites. *Polymer composites* 1997; 18: 16-27.
17. Castaings M, Cawley P. The generation, propagation, and detection of Lamb waves in plates using air-coupled ultrasonic transducers. *The Journal of the Acoustical Society of America* 1996; 100: 3070-3077.
18. Castaings M, Cawley P, Farlow R, Hayward G. Single sided inspection of composite materials using air coupled ultrasound. *Journal of Nondestructive Evaluation* 1998; 17: 37-45.
19. Castaings M, Hosten B. Lamb and SH waves generated and detected by air-coupled ultrasonic transducers in composite material plates. *Ndt & E International* 2001; 34: 249-258.
20. Kelly SP, Farlow R, Hayward G. Applications of through-air ultrasound for rapid NDE scanning in the aerospace industry. *Ultrasonics, Ferroelectrics and Frequency Control, IEEE Transactions on* 1996; 43: 581-591.
21. Chimenti D. Review of air-coupled ultrasonic materials characterization. *Ultrasonics* 2014; 54, 7: 1804–1816
22. Standard A. D7136/D7136M. Standard test method for measuring the damage resistance of a fiber-reinforced polymer matrix composite to a drop-weight impact event. West Conshohocken (PA): ASTM International, 2007: 1-16.
23. Sfondrini MF, Massironi S, Pieraccini G, Scribante A, Vallittu PK, Lassila LV, Gandini P. Flexural strengths of conventional and nanofilled fibre-reinforced composites: a three-point bending test, *Dental Traumatology*, 2014; 30: 32-35.
24. Shyr T-W, Pan Y-H. Impact resistance and damage characteristics of composite laminates. *Composite Structures* 2003; 62: 193-203.

Received 16.01.2014 Reviewed 31.03.2014